DOI: 10.1002/chem.200801019

Phase Transformation in Titania Nanocrystals by the Oriented Attachment Mechanism: The Role of the pH Value

Caue Ribeiro,*[a] Cristiano M. Barrado,[b] Emerson R. de Camargo,[b] Elson Longo,[c] and Edson R. Leite[b]

Abstract: A new synthetic method for TiO_2 nanocrystals starting from metallic Ti and hydrogen peroxide was developed, in order to obtain minimal interferences to evaluate phase transformation in the system. The results revealed that the crystal morphology appeared to be dictated by the pH value, which shows a strong dependence on the surface energy. The involvement of the oriented attachment (OA) mechanism is important to modify the morphology and, hence, the distribution of the surface energy and confirmed that the mechanism can accelerate certain phase transitions, albeit pH dependence in terms of how the mechanism affects the final particle morphology and direction of crystalline growth. The importance of the mechanism was also apparent in extremely basic conditions, which indicates a possible correlation with the formation of hydrogen titanate nanostructures.

Keywords: crystal growth · nanostructures · oriented attachment · phase transitions

Introduction

Nanoparticle growth mechanisms have received much attention in recent years, especially in view of the importance of controlling nanostructural sizes and morphologies. In-depth investigations into classical nanoparticle coarsening processes (Ostwald ripening: OR[1,2]) have demonstrated the importance of the control in this stage of the synthesis so that the desired nanostructures can be obtained.[3–5] However, an important nonclassical growth mechanism—commonly called the oriented attachment (OA) mechanism[6–9]—has been highlighted as a common step in nanocrystal growth, even in systems with high solubility (when OR is to be expected[10]).

The influence of this mechanism on the anisotropy of oxide nanocrystals has been investigated,[11–14] and a wide range of distinct nanostructures such as nanowires,[11,15] multipods,[16] nano-heterostructures[17,18] and other unusual shapes[19] are reportedly formed through this mechanism.

However, although the role of this mechanism in nanoparticle morphology is well understood, further investigations into other implications are still necessary. One aspect is the mechanism's influence on the phase control, an important variable, particularly in systems with many polymorphs, and one that is frequently disregarded. In general, many metastable structures appear to be stable in the nanometric range, without the addition of dopants or constriction by a matrix.[20] That is the case of TiO_2 synthesis, commonly observed as anatase in the nanometric range,[21–24] and ZrO_2, which is observed in tetragonal phase in sizes below 12 nm.[25]

A necessary generalization of the discussion is to assume that phase stability depends on global thermodynamic parameters, that is, the total surface energy of the particle as a function of the volume. A general expression for the free energy G_x^0 of an arbitrary nanoparticle, taking into account the balance of surface energy as a function of the exposed crystallographic planes, was proposed as follows:[26–31]

$$G_x^{0} = G_x^{bulk} + M/\rho_x\,(1-e)\,q\sum_i f_i\,\gamma_i(T) \qquad (1)$$

[a] Dr. C. Ribeiro
EMBRAPA Instrumentação Agropecuária
Rua XV de Novembro, 1452-13560-970, CP 741
São Carlos, SP (Brazil)
Fax: (+55) 16-2107-2902
E-mail: caue@cnpdia.embrapa.br

[b] Dr. C. M. Barrado, Prof. Dr. E. R. de Camargo, Prof. Dr. E. R. Leite
LIEC/Universidade Federal de São Carlos
Departamento de Química, Rod. Washington Luiz
km 235-13565-905, São Carlos, SP (Brazil)

[c] Prof. Dr. E. Longo
LIEC/Universidade Estadual Paulista
Instituto de Química, Rua Francisco Degni, s/n
14800-900, Araraquara, SP (Brazil)

Supporting information for this article is available on the WWW under http://dx.doi.org/10.1002/chem.200801019.

The first term defines the standard free energy of formation, $G_x^{bulk} = \Delta G_x^0(T)$, the second is expressed in terms of surface energy γ_i for each i plane on the surface and molar surface area A—which can be described using the relations of density of the phase $x(\rho_x)$, molar mass M, the volume dilation of the nanoparticle e (negligible in several cases), the surface to volume ratio q and f_i, a weight factor of the facets i in the crystal ($\Sigma f_i = 1$). This equation takes into account the crystallographic alignment of the particles and, indirectly, the shape or anisotropy. In this formulation, we can sum up the contributions of factors as the interaction with ions on the surface (counterions, surfactants, etc.) as a way to minimize energy in specific crystallographic planes.

In this discussion, the role of the growth mechanism in phase control can be understood in terms of its influence on the weight factor f_i of the facets, which can be attained by tailoring anisotropic structures (since the OA mechanism is related to this aspect). Its influence is interpreted as the modification of the area/volume relation in the particles formed, favoring phase transformation or not according to the crystallographic planes exposed after the reaction. However, the surface energy of each plane is strongly influenced by the presence of counterions in the medium. In the synthesis of TiO_2, it has been shown that the presence of common ions in the synthesis environment, such as Cl^- or organic chains from the precursors, can alter the phase stability.[32,33] Other influences in the media, such as microwave frequencies,[34] can also favor the growth, changing the path of the phase transformation. In order to obtain a representative system for TiO_2 with minimal interferences, we have developed a clean synthesis using metallic Ti and hydrogen peroxide as precursors, crystallized in a conventional hydrothermal apparatus. This system can offer some insights on the influence of surface energy in the OA mechanism and its importance for adequate phase control of nanoparticles during synthesis.

Results and Discussion

Figure 1 shows the X-ray diffraction patterns obtained under all the synthesized conditions, while Figure 2 shows the Raman shifts for the same samples. The two techniques revealed that hydrothermalization at pH 0 was the only condition in which the rutile phase was detected, and that only anatase was detected between pH 2–12. It is important to note that this behavior was confirmed with the Raman shifts, which are more sensitive to phase mixtures than XRD. This finding does not agree with previous results,[33] which describe the synthesis of rutile or rutile/anatase mixtures with several morphologies in pH <4. This highlights the importance of counterions in the system. The presence of organic counterions or halides may interfere in the surface energy by specific adsorption, favoring the rutile phase even at higher pH values.

In our system, even with a positive surface (in a pH below the isoelectric point) the adsorption of NO_3^- can not be the rate-determining step in the rutile formation. The results and observations describe above offer insight into the Ostwald step rule,[20] that is, the crystallization path to rutile necessarily passes through, at least, amorphous → anatase → rutile phases. This hypothesis could work if the rutile phase formation is associated with a more complicated pro-

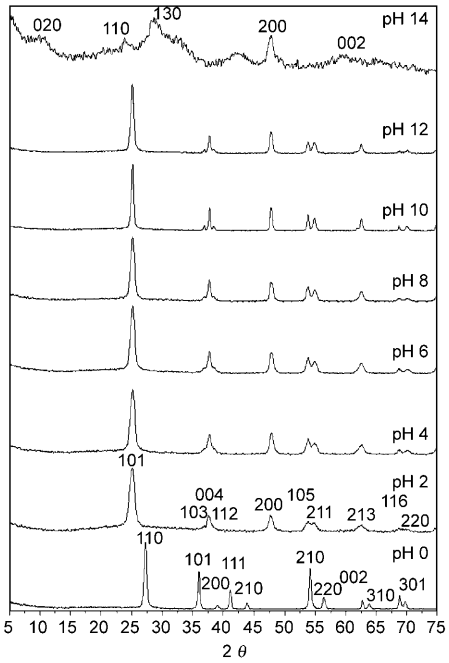

Figure 1. XRD patterns of the as-synthesized samples, showing the reflection attributed to rutile (pH 0), anatase (pH 2) and hydrogen titanate (pH 14).

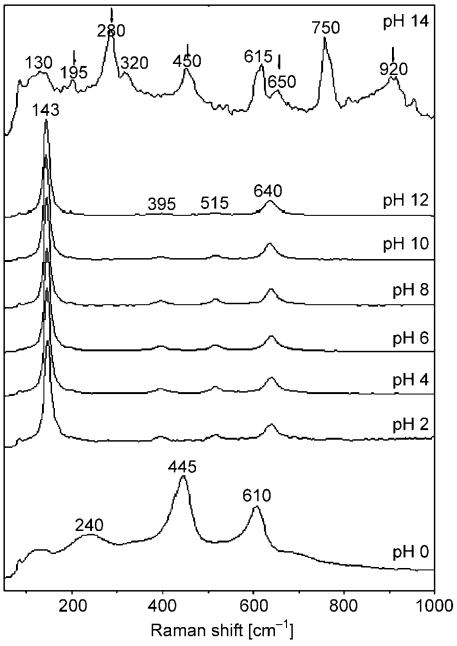

Figure 2. Raman shifts of the as-synthesized samples, showing the peaks attributed to rutile (pH 0) and anatase (pH 12). In pH 14, the peaks attributed to hydrogen titanate are marked by arrows.

cess than the attachment/detachment of small molecules or ions, such as oriented attachment of nanocrystals. However, this occurs only when the conditions of the media favor the coordination of positive counterions on the surface. This may indicate that the stabilization of rutile under such extreme conditions is related to surface contacts of preformed anatase nanoparticles, as previous suggested.[36,37]

Since the crystallographic coherence can be accepted as an indication of the particle size in each direction, the values calculated for each plane can also clarify our discussion, as shown in Table 1. The measurements of the rutile phase synthesized in pH 0 show slightly anisotropic nanoparticles, with larger sizes than those obtained in pH 2, which results in more uniform anatase nanoparticles. We would like to note the difference in sizes under the two conditions, since this confirms the correlation of rutile stabilization and crystal growth, as discussed in previous works.[33,37] The other values clearly indicate the influence of the pH medium in the growth and anisotropy: the particle sizes vary only slightly from pH 2 to 6, but show a tendency for anisotropic growth in (004) (parallel to (001)), which is evident at pH 8 and 10, leading to the formation of anatase nanorods.

Table 1. Crystallograpfic coherence of the synthesized TiO_2 nanoparticles, calculated from XRD data.

Rutile	pH 0	Anatase	pH 2	pH 4	pH 6	pH 8	pH 10	pH 12
(110)	21.5	(101)	8.3	9.2	10.8	11.7	23.1	19.3
(101)	29.5	(103)	–	–	–	–	24.3	30.1
(200)	17.9	(004)	12.4	13.5	16.9	20.6	52.5	27.5
(111)	25.3	(112)	–	-	–	–	25.5	23.6
(210)	25.4	(200)	8.9	11.3	11.4	11.4	31.4	19.7
(211)	28.0	(105)	9.3	13.8	14.8	15.7	44.2	26.0
(220)	18.6	(211)	8.8	9.3	10.4	11.2	27.3	16.6
(002)	33.7	(213)	6.7	8.9	10.2	12.0	29.2	19.1
(310)	18.0	(116)	–	13.4	14.3	15.9	47.4	21.8
(301)	21.6	(220)	–	9.1	9.9	10.6	23.2	17.2

In pH 12 other effects, probably relating to the dissolution of the pristine nanoparticles, led to particle size reduction during crystallization. However, once again, only anatase was observed, indicating that probably no precipitation occurred in the as-formed anatase nanoparticles. The solubilization and reprecipitation of amorphous nanoparticles is also probable at pH 14, as indicated in Figures 1 and 2. The results obtained are similar to the pattern and Raman shifts reported for hydrogen titanate nanotubes (commonly called titanium oxide nanotubes),[38] with several dislocations indicating a poorly formed phase.[39] Previous works described the synthesis of titanate nanotubes[38–41] under extremely basic solutions (NaOH concentrations higher than $5\,mol\,L^{-1}$). However, to the best of our knowledge, this is the first report of a similar process occurring in a medium that is not very basic, using KOH (the concentration employed was $0.1\,mol\,L^{-1}$). This is important, since it also clarifies the role of the pH in phase stabilization: the basic environment implied in the dissolution of the amorphous precursor phase, precipitating the hydrogen titanate. Based on the results presented here we cannot state that the intercalation of K^+ ions did not occur, as observed for Na^+ ions in the aforementioned publications. However, this intercalation is less probable, since K^+ ions are larger and were not detected in our elemental analysis of the materials (not shown here). These results also confirmed that the phase formation was strongly dominated by the pH value of the medium, since a minor change of the pH from 12 to 14 completely changed the observed phase.

This morphological evolution is plainly visible in the FEG-SEM images (Figures 3, 4 and Figure S1). Rutile nanorods are clearly visible at pH 0 (Figure 3a), with slight size variations, suggesting a homogeneous crystallization process. This finding contrasts with the morphologies observed at pH 2–8 (Figure S1), showing agglomerated materials with very fine particle sizes. The morphology is not very different in these conditions, but anatase nanorods are identified at pH 10 (Figure 4c). At pH 12, an acicular morphology (nanoneedle) with irregular surfaces is observed (Figure 4e). Finally, at pH 14, there is an irregular and shapeless morphology, not clearly identifiable (Supporting Figure S1). These results are congruent with those observed in the XRD and Raman analyses: the anisotropic shape expected at pH 0 and 10 was confirmed, and the irregularity of the acicular nanoribbons observed at pH 12 diminished the crystallographic coherence. At intermediary pH values, the fine morphology was consistent with the small particle sizes inferred from the XRD measurements, and the amorphous morphology was congruous with the dissolution and reprecipitation of a different phase at pH 14.

Some aspects of the phase transformation mechanism, however, can only be elucidated through HRTEM images, illustrated in Figure 3–5. As shown in Figure 3b, the rutile nanoparticles presented internal line dislocations that were correlated with the OA growth mechanism. The nanoribbons grew toward (110), as expected from previous studies.[33] The mechanism appears to act preferentially on longitudinal growth, causing the nanorod to grow towards (110), although lateral growth was not unusual, as indicated in Figure 3c, which illustrates the statistical nature of the oriented attachment. At pH 8, the OA mechanism is observed in anatase nanoparticles (Figure 4b) in the (001) direction, which is the growth direction of all anatase nanoribbons. This comparison is an interesting illustration of the role of surface energy in phase stabilization, as calculated by Barnard and Zapol,[27] that is, the (110) are the lower energy planes in rutile, which is consistent with their suggested predominance, minimizing the total surface energy of the rod (the nanorod sides are (110), as indicated in the figure). On the

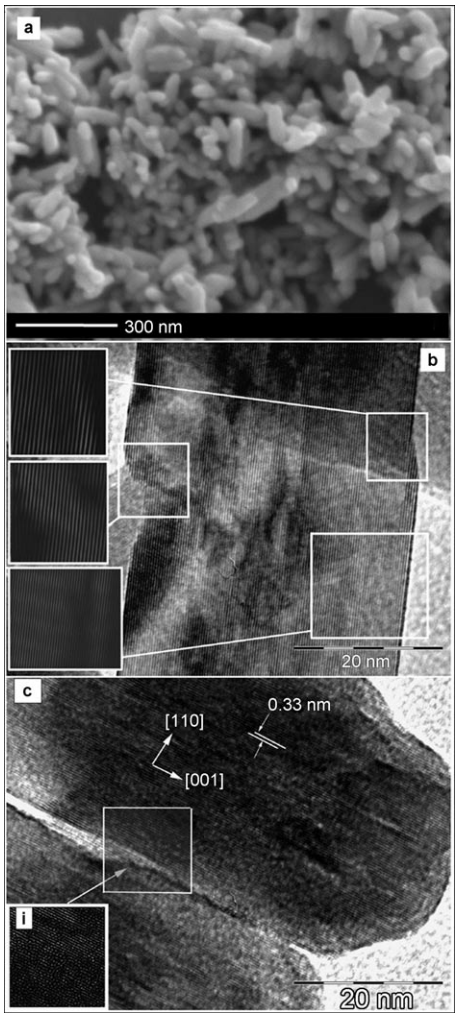

Figure 3. Images from representative samples: a) FEG-SEM image of rutile nanorods obtained in treatment at pH 0; b) HRTEM image of a rutile nanorod, showing line dislocations in the reconstructed lattice images in the insets; and c) HRTEM image of two laterally coalesced rutile nanorods, showing the reconstructed lattice in the inset.

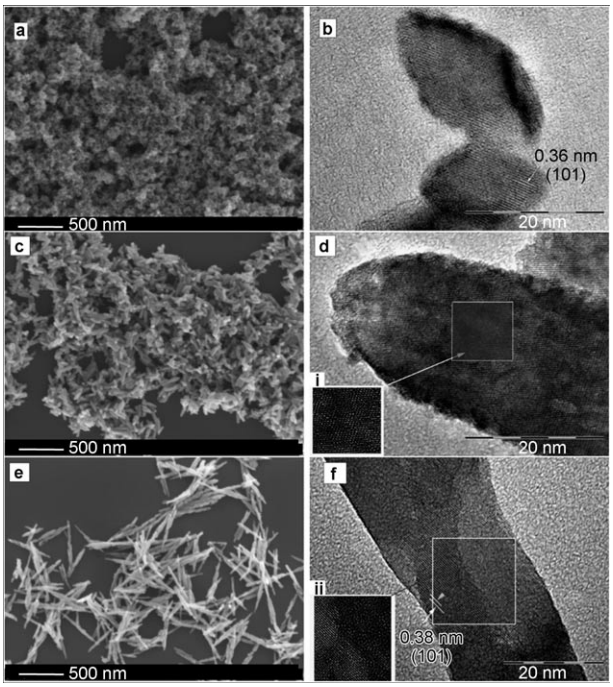

Figure 4. Images from representative samples: a) FEG-SEM image of anatase nanoparticles obtained in pH 8 and b) HRTEM image of the same sample, showing two anatase nanoparticles attached; c) FEG-SEM image of anatase nanorods obtained in pH 10 and d) HRTEM of the same sample; e) FEG-SEM image of anatase nanoneedles, obtained in pH 12 and f) HRTEM of the same sample. The insets in each image show the reconstructed lattice image of the selection.

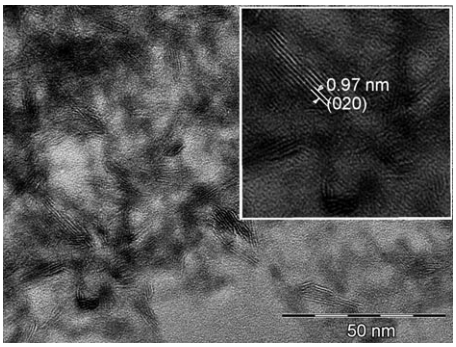

Figure 5. Images from representative samples: HRTEM image of titanate nanostructures obtained in pH 14, showing a detailed structure in the inset (the inset width corresponds to 50 nm).

other hand, the lower energy planes in anatase are (101). In fact, all conditions observed here showed the predominance of the plane family in the nanorods. In the synthesis at pH 8, the bypiramidal morphology was preserved in the coalesced nanoparticles, since (101) and (001) planes are not parallel; hence, the morphology could not stabilize on planar surfaces.

This feature is also depicted in Figure 4d, which shows a nanoribbon obtained in pH 10. In this case, the growth direction was the same as that observed in the other conditions, but the surface underwent a "smoothing" process, probably from concurrent OR to OA growth. However, note the surface roughness resulting from the large number of surface defects, probably residues from the pristine nanoparticles developed in the OA formation of the nanorod, which is evidenced by the line defects in the particle. In this case, the aggressive environment may have led to greater solubility, favoring the formation of larger nanoribbons. This assumption is supported by the morphology of the nanoparticles obtained at pH 12 (Figure 4f). The irregular morphology depicted here shows the dissolution of the particle in the points of attachment. This situation is coherent, since the density of defects at these points may be higher, so the solubility at these points must also be higher. Moreover, in this condition the structure assumes a planar attachment, illustrated in Figure 4f (see inset). This may indicate that few points on the surface are available for OA, with high coordination of OH on the other surfaces.

Finally, Figure 5 shows the competition occurring between OA and OR, where the pH 14 causes total dissolution of the previous structure and reprecipitation of the lamellar hydrogen titanate, as previously discussed. The interplanar spaces (see inset) were coherent with the (020) reflection, albeit with major deviations. As can be seen in the figure, the structure is irregular, presenting several defects such as line dislocations. Following Mao and Wong's hypothesis[38] for the phase transformation of hydrogen titanates to anatase nanostructures, since surface rearrangement is easier than complete solubilization and precipitation, it is probable that primary anatase nanoparticles that coalesced at specific points were altered to hydrogen titanate by reordering of the (101) plane in anatase to the (110) plane in titanate, which has a slight lattice mismatch. In this case, the line defects observed may have remained from attached contacts in pristine anatase nanoparticles. This hypothesis needs to be better evaluated, but it offers an interesting way to evaluate the formation of titanate nanotubes.

These results also demonstrate the importance of surface stabilization in the OA mechanism. OA occurred even in the case of the aggressive environment of pH 12, albeit in the high energy planes, that is, (001). In fact, Shannon and Pasks[42,43] noted that the anatase → rutile transformation would occur preferentially in systems where the Ti–O bonds are easily broken, as in an O_2-poor atmosphere at high temperatures. The same case is illustrated in very acid pH like the one used in our work. Also, since the same authors identified the transformation as topotactical, the results of our work lead us to conclude that the transformation is probably induced at the contact points during the OA of previously formed anatase nanoparticles. However, the evidence also shows that this is a weak condition in which a few surface variations can favor or prevent the transformation, highlighting the importance of surface energy in the role of the OA mechanism in the phase transformation of nanocrystals.

The results here lead to an important finding on the influence of the pH on the phase transformation process of titania nanocrystals. The growth mechanism is a quite complicated process, evolving a variety of attachment sites and local surface environments. In this way the role of the pH in the phase transformation is not simply an attachment/detachment of ions induced by pH change. The situation is more complicated and the OA mechanism of nanocrystal seems to be the rate-determining step process. The pH values modify the OA process and consequently it as important role in the phase transformation process.

Conclusion

In this work we developed a new synthesis method for TiO_2 nanocrystals, emphasizing clear conditions for a proper evaluation of their phase transformation and the correlation with the crystal's growth mechanism. The results revealed the evolution of the crystal morphology dictated by the conditions of pH, as summarized in Figure 6, which shows a strong dependence on the surface conditions, that is, surface energy—which is highlighted by the only condition in which rutile phase was stabilized (pH 0). The occurrence of the OA mechanism as an important way to modify the morphology and, hence, the distribution of surface energy, confirmed that the mechanism can accelerate some phase transitions, albeit with interference of the pH medium in terms of how the mechanism affects the final particle morphology and direction of crystalline growth. Finally, the importance of the mechanism was also apparent in an extremely basic condition, indicating a possible correlation with the formation of hydrogen titanate nanostructures. This may be the focus of future investigations.

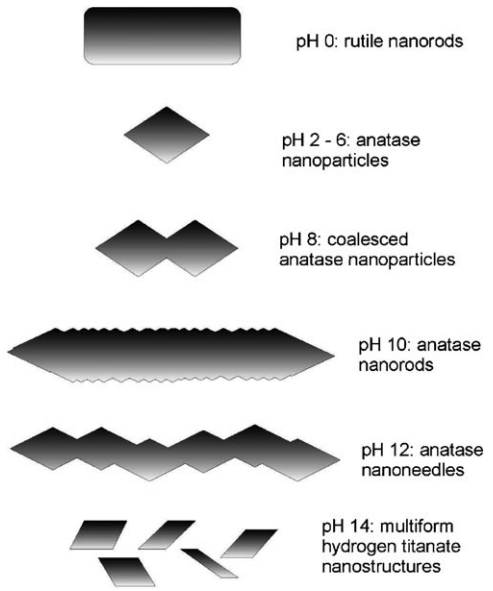

Figure 6. Graphical summary of the observed morphologies in this work.

Experimental Section

Titanium oxides were synthesized by the hydrothermal treatment of amorphous TiO_2 nanoparticles obtained from the peroxo complex of titanium (PCT) gel solution. The PCT gel was prepared by the digestion of metallic titanium powder in H_2O_2 solution. In a typical synthesis process, titanium metal powder (1 g, 0.02 mol) was added to an aqueous solution consisting of H_2O_2 and ammonia aqueous solution (20 mL). This solution was left in an ice-water bath for approximately 10 h, resulting in a yellow transparent aqueous solution of the soluble peroxytitanate $[Ti(OH)_3O_2]^-$ ion with a concentration of 0.14 mol L^{-1}. In order to obtain a pure amorphous precursor, the gel was degraded by rapid heating to 100 °C followed by immersion in an ice bath. A white precipitate corresponding to the amorphous precursor was formed, as confirmed in an x-ray diffraction analysis (not showed here). The suspension was kept under agitation for 24 h to release excess H_2O_2 and ammonia.

The amorphous precursor was redispersed in water, and pH was adjusted in the range 0–14 using HNO_3 or KOH. The acid, base were chosen to minimal interference in the synthesis environment: the dispersed NO_3^- and K^+ counterions are larger than the most common Cl^- or Na^+ counterions, and little adsorption in the as-formed crystalline TiO_2 nanoparticles was expected. The resulting suspensions were hydrothermallized at

200 °C for 2 h in a controlled reactor (Nanox Hidrocell model H100) to crystallize the material.

The X-ray diffraction patterns were obtained with a Rigaku D-Max 2500 diffractometer with $Cu_{K\alpha}$ radiation, in a scanning routine of 1 min, to define the peak position and width. Crystallographic coherence lengths were calculated according to Scherrer's equation,[35] deconvoluting each peak using a Lorentzian approximation to determine the full width at half maximum (FWHM) and using as reference FWHM the (101) reflection of a monocrystalline Silicon wafer. Raman spectra were collected at room temperature in a frequency range of 100 to 1000 cm^{-1} using a FT-Raman Bruker RFS 100/S spectrometer operating with the 1064 nm line of an yttrium aluminum garnet laser. The morphology of the systems was characterized with a field emission gun–scanning electron microscope (STEM FESEM, Zeiss Supra 35, at 1.5 kV) and a 200 kV transmission electron microscope (Philips CM200, IQ-UNESP facility). The TEM samples were prepared by wetting carbon-coated copper grids with a drop of the colloidal suspensions for 20 s, followed by drying in air.

Acknowledgement

The authors gratefully acknowledge the financial support of the Brazilian research funding agencies FAPESP and CNPq.

[1] I. M. Lifshitz, V. V. Slyozov, *J. Phys. Chem. Solids* **1961**, *22*, 35–50.
[2] C. Z. Wagner, *Z. Elektrochem.* **1961**, *65*, 581–591.
[3] V. F. Puntes, K. M. Krishnan, A. P. Alivisatos, *Science* **2001**, *291*, 2115–2117.
[4] G. Oskam, Z. S. Hu, R. L. Penn, N. Pesika, P. C. Searson, *Phys. Rev. E* **2002**, *66*, 011403-1-4.
[5] Y. Yin, A. P. Alivisatos, *Nature* **2005**, *437*, 664–670.
[6] R. L. Penn, J. F. Banfield, *Am. Mineral.* **1998**, *83*, 1077–1082.
[7] R. L. Penn, J. F. Banfield, *Science* **1998**, *281*, 969–971.
[8] C. Ribeiro, E. J. H. Lee, T. R. Giraldi, R. Aguiar, E. Longo, E. R. Leite, *J. Appl. Phys.* **2005**, *97*, 024313–1–4.
[9] M. Niederberger, H. Colfen, *Phys. Chem. Chem. Phys.* **2006**, *8*, 3271–3287.
[10] A. Ratkovich, R. Penn, *J. Phys. Chem. C* **2007**, *111*, 14098–14104.
[11] K. S. Cho, D. V. Talapin, W. Gaschler, C. B. Murray, *J. Am. Chem. Soc.* **2005**, *127*, 7140–7147.
[12] E. J. H. Lee, C. Ribeiro, E. Longo, E. R. Leite, *J. Phys. Chem. B* **2005**, *109*, 20842–20846.
[13] C. Ribeiro, E. J. H. Lee, E. Longo, E. R. Leite, *ChemPhysChem* **2005**, *6*, 690–696.
[14] C. Ribeiro, E. J. H. Lee, E. Longo, E. R. Leite, *ChemPhysChem* **2006**, *7*, 664–670.
[15] J. H. Yu, J. Joo, H. M. Park, S. I. Baik, Y. W. Kim, S. C. Kim, T. Hyeon, *J. Am. Chem. Soc.* **2005**, *127*, 5662–5670.
[16] D. Zitoun, N. Pinna, N. Frolet, C. Belin, *J. Am. Chem. Soc.* **2005**, *127*, 15034–15035.
[17] Q. Zhang, X. Chen, Y. Zhou, G. Zhang, S.-H. Yu, *J. Phys. Chem. C* **2007**, *111*, 3927–3933.
[18] C. Ribeiro, E. Longo, E. R. Leite, *Appl. Phys. Lett.* **2007**, *91*, 103105.
[19] Z. Tang, Y. Wang, S. Shanbhag, M. Giersig, N. Kotov, *J. Am. Chem. Soc.* **2006**, *128*, 6730–6736.
[20] A. Navrotsky, *Proc. Natl. Acad. Sci. USA* **2004**, *101*, 12096–12101.
[21] E. A. Barringer, H. K. Bowen, *Langmuir* **1985**, *1*, 414–420.
[22] L. Kavan, K. Kratochvilova, M. Gratzel, *J. Electroanal. Chem.* **1995**, *394*, 93–102.
[23] T. J. Trentler, T. E. Denler, J. F. Bertone, A. Agrawal, V. L. Colvin, *J. Am. Chem. Soc.* **1999**, *121*, 1613–1614.
[24] G. Garnweitner, M. Antonietti, M. Niederberger, *Chem. Commun.* **2005**, *3*, 397–399.
[25] R. C. Garvie, *J. Phys. Chem.* **1965**, *69*, 1238–1243.
[26] A. S. Barnard, P. Zapol, *J. Phys. Chem. B* **2004**, *108*, 18435–18440.
[27] A. S. Barnard, P. Zapol, *Phys. Rev. B* **2004**, *70*, 235403–1–13.
[28] A. S. Barnard, P. Zapol, *J. Chem. Phys.* **2004**, *121*, 4276–4283.
[29] A. Barnard, Z. Saponjic, D. Tiede, T. Rajh, L. Curtiss, *Rev. Adv. Mater. Sci.* **2005**, *10*, 21–27.
[30] A. S. Barnard, P. Zapol, L. A. Curtiss, *J. Chem. Theory Comput.* **2005**, *1*, 107–116.
[31] A. S. Barnard, R. R. Yeredla, H. Xu, *Nanotechnology* **2006**, *17*, 3039–3047.
[32] C. Kormann, D. W. Bahnemann, M. R. Hoffmann, *J. Phys. Chem.* **1988**, *92*, 5196–5201.
[33] C. Ribeiro, C. Vila, D. B. Stroppa, J. Bettini, V. R. Mastelaro, E. Longo, E. R. Leite, *J. Phys. Chem. C* **2007**, *111*, 5871–5875.
[34] M. Godinho, C. Ribeiro, E. Longo, E. R. Leite, *Cryst. Growth Des.* **2008**, *8*, 384–386.
[35] B. D. Cullity, Elements of X-Ray diffraction; Addison-Wesley, **1978**.
[36] A. A. Gribb, J. F. Banfield, *Am. Mineral.* **1997**, *82*, 717–728.
[37] C. Ribeiro, C. Vila, J. M. E. Matos, J. Bettini, E. Longo, E. R. Leite, *Chem. Eur. J.* **2007**, *13*, 5798–5803.
[38] Y. B. Mao, S. S. Wong, *J. Am. Chem. Soc.* **2006**, *128*, 8217–8226.
[39] H.-H. Ou, S.-L. Lo, *Sep. Purif. Technol.* **2007**, *58*, 179–191.
[40] G. H. Du, Q. Chen, R. C. Che, Z. Y. Yuan, L.-M. Peng, *Appl. Phys. Lett.* **2001**, *79*, 3702–3704.
[41] M. Cortes-Jacome, G. Ferrat-Torres, L. F. Ortiz, C. Angeles-Chavez, E. Lopez-Salinas, J. Escobar, M. Mosqueira, J. Toledo-Antonio, *Catal. Today* **2007**, *126*, 248–255.
[42] R. D. Shannon, J. Pask, *Am. Mineral.* **1964**, *49*, 1707–1717.
[43] R. D. Shannon, J. A. Pask, *J. Am. Ceram. Soc.* **1965**, *48*, 391–398.

Received: May 27, 2008
Revised: September 5, 2008
Published online: January 13, 2009

